EUROPEAN ORGANIZATION FOR NUCLEAR RESEARCH

CERN-EP/84-124
14 September 1984

PHOTOPRODUCTION OF MULTIPARTICLE STATES IN THE BEAM FRAGMENTATION REGION FOR PHOTON ENERGIES IN THE RANGE 50-70 GeV

Bonn[1]-CERN[2]-Glasgow[3]-Lancaster[4]-Manchester[5]-
Paris VI[6]-Rutherford[7]-Sheffield[8] Collaboration

(The Omega-Photon Collaboration)

M. Atkinson[7], T.J. Axon[5], D. Barberis[5], T.J. Brodbeck[4],
G.R. Brookes[8], J.J. Bunn[8], P.J. Bussey[3], A.B. Clegg[4],
J.B. Dainton[3], M. Davenport[7], B. Dickinson[5], B. Diekmann[1],
A. Donnachie[5], R.J. Ellison[5], P. Flower[7], P.J. Flynn[4],
W. Galbraith[8], K. Heinloth[1], R.C.W. Henderson[4],
R.E. Hughes-Jones[5], J.S. Hutton[7], M. Ibbotson[5], H.P. Jakob[1],
M. Jung[1], M.A.R. Kemp[7], B.R. Kumar[7], J. Laberrigue[6],
G.D. Lafferty[5], J.B. Lane[5], J.C. Lassalle[2], J.M. Lévy[6],
V. Liebenau[1], R.H. McClatchey[8], D. Mercer[5], J.A.G. Morris[7],
J.V. Morris[7], D. Newton[4], C. Paterson[3], G.N. Patrick[2],
E. Paul[1], C. Raine[3], M. Reidenbach[1], H. Rotscheidt[1],
A. Schlösser[1], P.H. Sharp[7], I.O Skillicorn[3], K.M. Smith[3],
K.M. Storr[2], R.J. Thompson[5], Ch. de la Vaissière[6],
A.P. Waite[5], M.F. Worsell[5] and T.P. Yiou[6]

ABSTRACT

Forward production of hadrons in γp interactions at about 11 GeV. Centre of mass energy has been analysed in terms of single particle spectra. Comparisons with K^+p and K^-p data with deep inelastic scattering data at similar energies confirms the universality of global properties. As the minimum p_T^2 is increased the data show features which are consistent with a two-jet structure in the beam fragmentation region. A small subsample of these events is consistent with a special topology in which a jet is replaced by a single high-p_T pion.

(Submitted to Zeitschrift für Physik C)

1. INTRODUCTION

A consistent qualitative picture of jets and parton fragmentation has been developed in e^+e^- annihilation, deep inelastic scattering and hard hadron-hardon scattering. Further, there is increasing evidence for similarities between jets in soft hadronic interactions and those observed in e^+e^- annihilation when compared at the same total hadronic energy [1-4].

In most respects, one anticipates that high-energy photon interactions will be very similar to high-energy hadron interactions through the concepts of vector meson dominance. However, at some level significant differences should appear due to the point-like interaction of the real photon. Specifically, in high-energy photoproduction one expects to see "three-jet" events, which consist of a target jet and two opposed high-p_T jets in the beam fragmentation region with no particles in the beam direction. These arise from the QCD Bethe-Heitler process of Fig. 1, in which a quark and an antiquark are produced at large transverse momentum, and the QCD Compton process of Fig. 2 with a quark (or antiquark) and a gluon jet. These processes could account for a few percent of the total cross-section at high energies.

In principle, a similar signature can be obtained through vector dominance, the vector meson coupling directly to two high-p_T jets, Fig. 3, analogously to the higher twist process $\pi q \to gq$ in which the pion couples directly to two high-p_T jets [5]. However, this higher twist process is predicted to have a smaller cross-section than the minimum twist QCD Bethe-Heitler and Compton processes, and should not produce a significant contribution to any "three-jet" signal.

Of more immediate interest is the higher twist process of Fig. 4 which involves the point coupling of the real photon. A quark and antiquark combine into a single high-p_T meson ($\pi,\rho,\ldots$) with a balancing jet [6]. Although the cross-section is calculated to be appreciably smaller than the QCD Bethe-Heitler and Compton cross-sections, each event from the higher-twist process should have one particle carrying all the transverse momentum on one side of a "three-jet" event. Unfortunately this signature is not unique. For example, in a certain fraction of events the QCD Bethe-Heitler and Compton processes will produce a single high-p_T hadron through a high-z parton fragmentation.

In this paper we present a comparison of γp interactions at $\langle\sqrt{s}\rangle$ = 10.6 GeV with K^+p interactions at $\sqrt{s}$ = 11.5 GeV [4], K^-p interactions at $\sqrt{s}$ = 14.3 GeV [3], and deep inelastic muon scattering at $\langle\sqrt{s}\rangle$ = = 10.5 GeV [7], which confirms the general characteristics of hadron production in all the processes. As the minimum $\Sigma_i (p^i_{T_{in}})^2$ is increased (where $p^i_{T_{in}}$ is the component of the transverse momentum in the event plane), the data show the emergence of a "three-jet" structure. Further, a small subset of the "three-jet" sample consists of events with a single high-p_T pion balanced by a multiparticle jet.

2. EXPERIMENT AND DATA SAMPLE

An 80 GeV electron beam from the CERN SPS was used to produced tagged photons of energy 20–70 GeV [8], which were incident on a liquid hydrogen target 600 mm long. The particles produced were detected in the Omega spectrometer and in a large aperture photon detector. A description of the experimental set-up can be found elsewhere [9]. The trigger for the events discussed in this paper required a minimum incident photon energy of 50 GeV and at least three charged particles in a forward MWPC. Electromagnetic background was reduced by a system of veto counters in the median plane. Pattern recognition and geometrical reconstruction of events were performed by the program TRIDENT [10], and neutral pions were reconstructed from the signals in the photon detector.

The initial data sample used consisted of 373 K events. Events containing badly measured tracks were excluded from the analysis, and the final sample was further reduced by demanding charge balance, i.e. requiring a net charge of 1 or 0. We have checked that the physics results are not changed by this latter cut. Finally events compatible with being due to the diffractive dissociation of the photon to ρ, ω were removed. Together these cuts reduced the data sample to 131 K events.

In a large fraction of the events, the total energy measured in the Omega spectrometer and the photon detector was less than the initial beam energy. The detection angle of neutral pions and photons was limited by the geometry of the photon detector and the detection efficiency for slow charged tracks was low, partly due to absorption in the hydrogen target and partly due to restricted coverage at wide angles. These limitations meant

that a substantial fraction of the target fragments were not detected. This is most clearly demonstrated in the overall γp centre of mass. Figure 5 shows the missing longitudinal momentum (i.e. along the incident beam direction) in the overall γp centre of mass. The substantial loss in the target fragmentation region is obvious. It is worth noting that at the mean photon energy of 59 GeV, the backward hemisphere in the γp centre of mass corresponds to particles having less than 1 GeV longitudinal momentum in the laboratory. The average value of the missing longitudinal momentum is $\langle p_L \rangle = -2.47$ GeV/c.

The missing transverse momentum (i.e. perpendicular to the incident beam direction) is shown in Fig. 6. The average value of the missing transverse momentum is $\langle p_T \rangle = 0.53$ GeV/c. A two-dimensional plot of missing p_T v. missing p_L (not shown) demonstrates a strong correlation between large missing transverse momentum and large missing longitudinal momentum in the backward hemisphere, i.e. they correspond to slow, wide-angle tracks in the laboratory. This result is not surprising, since the Omega spectrometer has good acceptance for charged particles for $x_F > 0$ at the energies with which we are concerned, and the photon detector efficiency is also high for photons with positive x_F.

3. ANALYSIS PROCEDURE

Since our primary interest is in the beam fragmentation region, the loss of some target fragments does not present too serious a problem, although it does preclude a full thrust or sphericity analysis. The procedure adopted was to use a modified sphericity analysis. The data were analysed on an event by event basis, in each case finding the event axis [that direction with respect to which $\Sigma_i (p_T^i)^2$ is a minimum] and the event plane [that plane with respect to which $\Sigma_i (p_{T_{out}}^i)^2$ is a minimum]. The axis obtained is equivalent to the sphericity axis and it is distributed in a small cone about the beam direction, Fig. 7. Note that the K^+p analysis [4] at $\sqrt{s} = 11.5$ GeV was done in terms of sphericity, spherocity and thrust, with no change in the conclusions, so our choice of sphericity should not affect our conclusions.

An alternative and simpler approach would have been to assume that the correct axis is the beam axis. This is the approach which is adopted, for

example, in equivalent analyses of deep inelastic muon scattering data [7,11]. A simialr procedure has been investigated here to the point of demonstrating that the main qualitative features are unchanged, although distributions are naturally smeared in comparison with the sphericity axis analysis. Unless specified otherwise, all distributions shown and discussed relate to the sphericity axis procedure.

In performing the sums over momenta in the analysis it is necessary to specify which momenta to include, i.e. whether to retain charged tracks only or whether to incorporate measured neutrals as well. Both possibilities have been explored, with no significant difference between the results in the two cases. All results presented relate to the case where measured neutrals were included in the determination of the event axis.

The immediate results of this analysis procedure are shown as the black circles in Figs. 8 and 9. Figure 8 is the inclusive single charged particle p_T^2 distribution with respect to the sphericity axis and Fig. 9 shows the distributions $\Sigma_i (p^i_{T_{out}})^2$ and $\Sigma_i (p^i_{T_{in}})^2$ with respect to the event plane for charged particles, "out" and "in" having their obvious meanings. In each case only charged tracks with $x_F > 0$ are included because of the problems associated with target fragmentation, and the restriction to charged tracks only is to allow direct comparison with other data.

4. RESULTS

4.1 Single particle distributions

As a first step, we compare our inclusive single particle distributions in Figs. 8 and 9 with the corresponding data from hadronic interactions at similar energies, namely K^+p at 70 GeV/c [4] and K^-p at 110 GeV/c [3], and with a subset of deep inelastic scattering data in the range $40 \leq s \leq 180$ GeV^2 [7]. The K^+p and K^-p data have been extensively compared [3,4] with e^+e^- data in the range $13 \leq \sqrt{s} \leq 17$ GeV [11] and with νN data in the range $12 < \sqrt{s} < 14$ GeV [12] and exhibit essentially the same features.

Our inclusive single-particle p_T^2 distribution is compared with the corresponding distributions from the K^+p [4] and K^-p [3] data in Fig. 8.

Clearly the distributions are similar. Unfortunately the hadronic data do not go beyond $p_T^2 = 2$ (GeV/c)^2 so a comparison at high p_T^2 is not practicable. Our distributions of $\Sigma_i(p^i_{T_{out}})^2$ and $\Sigma_i(p^i_{T_{in}})^2$ are compared with the corresponding distributions from the K^-p data [3] and from the appropriate subset of μp data [7] in Fig. 9. Once again the distributions are similar. The apparent difference between our "out-of-plane" data and the corresponding μp data [7] is not significant, being within the uncertainties coming from choosing the beam axis as the event axis in the latter case.

It is known [3] that in Kp interactions these distributions show a strong energy dependence between centre of mass energies of 4.5 and 14.3 GeV. The tail of the single particle p_T^2 distribution rises rapidly with increasing energy and the $\Sigma_i(p^i_{T_{in}})^2$ distribution develops a noticeable tail at high p_T^2. These phenomena are well known in e^+e^- [12], μp [7,11] and νp [14] reactions, and are usually ascribed to the onset of hard gluon effects. There is no universal agreement as to their origin in the hadronic interactions, although it is certainly the case that they cannot be described [3] by a simple fragmentation or longitudinal phase space model. The data are more planar, i.e. the $\Sigma_i(p^i_{T_{in}})^2$ distribution has a longer tail, than can be accommodated in these models without some addition analogous to the hard gluon effects in the leptonic interactions.

Whatever the source of these tails in the p_T^2 and the $\Sigma_i(p^i_{T_{in}})^2$ distributions in hadronic interactions, the important question from our immediate point of view is whether the rise in these tails with increasing energy continues beyond 14.3 GeV or whether saturation sets in. The fact that the photon data at $\sqrt{s}$ = 10.6 GeV are certainly as hard as the Kp data at $\sqrt{s}$ = 11.5 GeV and at $\sqrt{s}$ = 14.3 GeV could mean that saturation has indeed set in. On the other hand, it could mean that there is still some energy dependence with the p_T^2 distribution in photon interactions lying on a higher curve than that for hadron interactions. The only hadronic data available at higher energies comes from ISR analyses of the mesonic subsystem from pp interactions with the leading protons removed [1,2]. Basile et al. [1] claim evidence for energy dependence of the high p_T tail, but the more detailed analysis of Breakstone et al. [2] appears to show no variation between the two regions $11 < M_o < 18$ GeV and $30 < M_o <$ < 35 GeV, where M_o is the invariant mass of the mesonic subsystem. However

the inclusive single particle distribution from the latter analysis of the mesonic subsystem with M_o between 11 and 18 GeV is markedly different from the corresponding distribution in K^-p interactions at 14.3 GeV centre of mass energy, so the relevance of the ISR analyses to our present discussion is not clear.

The most direct evidence for saturation is probably that from the separate analysis of the forward and backward hemispheres in full acceptance neutrino experiments [14]. The mean single particle p_T^2 from that analysis is shown as a function of $\sqrt{s}$ in Fig. 10, together with the result of the present analysis (which is in the forward hemisphere). The backward data, which are presumably not describable by low-order QCD, do indeed appear to saturate (at least in this particular variable) and the separation between the forward and backward data occurs in the region of 10 GeV centre of mass energy, i.e precisely at the energy of this photon experiment. It is worth noting in this context that K^+p interactions at $\sqrt{s}$ = = 11.5 GeV [4] show evidence of symmetry in $\langle p_T^2 \rangle$ as a function of x_F in the forward and backward hemispheres, with the forward hemisphere possibly showing some slight broadening. However, the presence, or absence, of a baryon does not appear to have any significant effect on $\langle p_T^2 \rangle$ at this energy. It is quite clear that as far as the distributions we have studied are concerned, there is no real distinction between νN, Kp and γp reactions at the energies which we are considering.

However, the x_F distribution of $\langle p_T^2 \rangle$ for this photon experiment does appear to be somewhat different from that for the K^+p reactions. The comparison is made in Fig. 11. Although the distributions are qualitatively the same, e.g. both show the seagull effect, the photon data appear to be distinctly harder in the region of $x_F = 0$. Whether this points to a genuine difference in the underlying physics or whether it is merely a consequence of the different quark content of the beams is unknown. The apparent difference at high x_F is much less significant because of the different charged particle multiplicities. Integrated over all x_F, $\langle p_T^2 \rangle$ (or $\langle p_T \rangle$) in the two cases is essentially the same, as was already apparent from Fig. 8.

4.2 Energy flow distributions

It is apparent from the above discussion that any differences among the different reactions are ones of detail. The particular one in which we are interested is energy flow with respect to the event axis in the event plane, since three-jet events (if present) should show a double peaked structure. It is worth recalling the EMC results at $\langle\sqrt{s}\rangle \simeq 10$ and 16 GeV [7,11]. At the higher energy, including all events gave a symmetrical energy flow distribution peaked along the axis: cutting on p_T^2 in the event plane [the actual cut was one particle with $p_T^2 > 2$ (GeV/c)^2] gave a clear double distribution which was interpreted as two parton jets (mainly quark plus hard gluon). The data from the present experiment are shown in Fig. 12, where the cuts are on $\Sigma_i (p_{T_{in}}^i)^2 > p_{T_{min}}^2$, with $p_{T_{min}}^2$ successively 0 (i.e. all events included), 1, 2, 3 (GeV/c)^2. The fraction of all events contained in Figs. 12b, 12c, and 12d are, respectively, 18%, 2.6%, and 0.5%.

It is quite unambiguous that as the total p_T^2 in the data is increased, a double-peaked structure emerges and becomes more and more evident. In any one event there is always a 'harder' jet and a 'softer' jet, and in some analyses the 'harder' jets have been overlaid on each other to produce an asymmetrical distribution. This has not been done here, and so the resultant distributions are symmetric about the event axis: the two halves could be overlaid without loss of content.

Equivalent energy flow distributions have been given for the K^+p data at $\sqrt{s}$ = 11.5 GeV [4], the cut in that case being on decreasing thrust (which is equivalent to increasing the total p_T^2). These distributions also develop a dip on the axis as thrust is decreased, and they are qualitatively similar to the ones obtained here. Although the use of different variables precludes a quantitative comparison, the off-axis peak in the K^+p data appears to be less marked than in the γp case.

The curve in Fig. 12d shows the energy flow expected from the QCD Compton and Bethe-Heitler processes, assuming that the invariant mass of the qq or qg system is greater than 2.0 GeV, that the invariant momentum transfer from the initial photon to the quark is greater than 1.0 (GeV/c)^2 and that the quark and gluon fragmentation can be adequately described by

simple longitudinal phase space. The calculated cross-section for the QCD Compton and Bethe-Heitler processes for the events of Fig. 12d is 250 nb, assuming $\alpha_s = 0.25$ and applying the above kinematical cuts. This is comparable to the observed rate. This calculation is illustrative only, since the detailed results do depend on the choice of minimum invariant mass and momentum transfer. Nonetheless the calculation is sufficient to show that the γp results can be interpreted in terms of a contribution from the expected three-jet events (which we recall could amount to a few percent of the total cross-section) in addition to a flatter distribution from normal hadron-like events. However this interpretation is clearly not unique and only a direct comparison with equivalent hadron data can provide an explicit test.

4.3 High p_T single particles

The distribution of the number of particles in the individual "jets" (i.e. the particle clusters on either side of the event axis in the beam fragmentation region) is shown in Fig. 13 for the same cuts on $\Sigma_i (p^i_{T_{in}})^2$ as in Fig. 12. A fraction of the jets consists of one charged particle, this fraction increasing from less than 2% for all events to 7.6% for events with $\Sigma_i (p^i_{T_{in}})^2 > 3$ (GeV/c)^2. The p_T^2 distribution of these "single-particle jets" is given in Fig. 14, summed over all x_F, and their x_F distribution is given in Fig. 15, summed over all $p_T > 1$ GeV/c. A two-dimensional plot (not given) shows that high p_T is correlated with small x_F.

There are at least three possible sources of these single-particle jets. One is higher twist (Fig. 4), a second is high-z parton fragmentation (Figs. 1 and 2) of the QCD Bethe-Heitler and Compton processes and a third is a single particle from the tail of the normal hadron distribution. The last is not calculable, but reasonable estimates can be made for the first two.

The higher twist calculation is straightforward assuming that all charged particles are pions. Using the standard dipole Q^2 dependence for the pion form factor gives the solid curve shown on Figs. 14 and 15. (The normalization is arbitrary.) All possible proton valence and sea quark contributions have been included. In the calculation of the minimum twist

QCD Bethe-Heitler and Compton processes, it is necessary to make some assumption about the amount of high-z fragmentation which should be included. We have assumed that if, after fragmentation, the residual momentum is less than the mean transverse momentum (i.e. 350 MeV/c) then the remaining particle(s) in the fragmentation could be erroneously ascribed to the other jet and the high-z particle could appear by itself. On the other hand, if the residual momentum after fragmentation is greater than this, then we would expect to see two (or more) particles together. For simplicity we used the quark fragmentation functions of Field and Feynman [15], assumed that gluon fragmentation is the same as quark fragmentation and for the QCD Compton process included all possible proton valence and sea quark contributions. With these assumptions, the contribution from high-z fragmentation is less than 25% of the higher-twist contribution. However this result depends critically on the assumption of 350 MeV/c as the longitudinal momentum cut-off. Because of the slope of the high-z fragmentation function, small changes in the high-z cut-off have a major effect on the normalization, although the effect on the shape is less marked. The result of the minimum-twist calculation (using the 350 MeV/c cut-off) is shown as the broken line in Fig. 15 normalized with respect to the higher-twist calculation.

It is clear that the higher-twist model provides an adequate description of the data as regards the shape of both the x_F and the p_T distributions. Further the expected cross-section is the same order of magnitude as that observed, which is in the region of 15-20 nb. This is perhaps somewhat larger than the precise expectations of higher twist, which lie in the 5-10 nb range, but it is clear from the above discussion that any difference can be incorporated into high-z fragmentation.

5. CONCLUSIONS

We have demonstrated that the global features of γp reactions at $\sqrt{s}$ = 10.6 GeV are compatible with those of K^+p, K^-p, μp, and νp reactions at similar centre of mass energies. This is to be expected because we know that the perturbative QCD modifications to the leptonic processes do not become apparent until higher centre of mass energies and we expect any point-like behaviour of the real photon to contribute at most a few percent of the total γp cross-section.

A more detailed comparison of the γp data with K^+p data at $\sqrt{s}$ = 11.5 GeV shows two possible differences. There is some indication that $\langle p_T^2 \rangle$ near $x_F = 0$ is larger for γp reactions than for K^+p and that the energy flow distribution in γp is more peaked off-axis than in K^+p. Neither result is conclusive, but both are effects which would be expected from the point-like interaction of the real photon superimposed on its dominant hadron-like behaviour.

An interesting feature is the existence of "one-particle jets" in a way which is reasonably consistent with QCD expectations. Hadron data have unfortunately not been analysed in this way, so whether these events represent a genuinely unique feature of photon interactions or merely arise from the tail of the normal hadron distribution is unknown.

REFERENCES

[1] M. Basile et al., Phys. Lett. 93B (1980) 367; Nuovo Cimento 58A (1980) 193; Phys. Lett. 95B (1980) 311; Lett. Nuovo Cimento 29 (1980) 491.

[2] A. Breakstone et al., Z. Phys. C11 (1981) 203.

[3] R. Göttgers et al., Nucl. Phys. B206 (1982) 349 and B178 (1981) 392.

[4] M. Barth et al., Nucl. Phys. B192 (1981) 289.

[5] E. Berger and S.J. Brodsky, Phys. Rev. D24 (1981) 2428.

[6] J.A. Bagger and J.F. Gunnion, Phys. Rev. D25 (1982) 2287.

[7] H.E. Montgomery, CERN-EP/81-137 and CERN-EP/82-192.

[8] D. Aston et al., Nucl. Instrum. Methods 197 (1982) 287.

[9] Experiments at CERN in 1980 (CERN, Geneva, 1980): experiment WA57.

[10] J.C. Lassalle, F. Carena and S. Pensotti, Nucl. Instrum. Methods 176 (1980) 371.

[11] J.J. Aubert et al., Phys. Lett. 100B (1981) 433.

[12] R. Brandelik et al., Phys. Lett. 86B (1979) 243.

[13] K.W.J. Barnham et al., Phys. Lett. 85B (1979) 300.

[14] H.C. Ballagh et al., Phys. Rev. Lett. 47 (1981) 556.

[15] R.D. Field and R.P. Feynman, Nucl. Phys. B136 (1978) 1.

Figure captions

Fig. 1 : The QCD Bethe-Heitler process in γp reactions.

Fig. 2 : The QCD Compton process in γp reactions.

Fig. 3 : Hadron-like higher-twist contribution to three-jet events in γp reactions.

Fig. 4 : Higher-twist contribution giving a single particle at high p_T in γp reactions.

Fig. 5 : Missing longitudinal momentum in γp centre of mass.

Fig. 6 : Missing transverse momentum in γp centre of mass.

Fig. 7 : Distribution of angle between the sphericity axis and beam axis.

Fig. 8 : Inclusive single charged particle p_T^2 distribution in the beam fragmentation region, with respect to the sphericity axis. The present data (●) are compared with the corresponding data in K^+p [4] (o) and K^-p [3] (□) reactions.

Fig. 9 : $\Sigma_i (p_T^2)^2$ single charged particle distributions "in" and "out" of the event plane, in the beam fragmentation region. The present data (●) are compared with the corresponding data in μp [7] (o) and K^-p [3] (□) reactions.

Fig. 10 : Comparison of $\langle p_T^2 \rangle$ from this experiment (●) for the forward hemisphere (i.e. beam fragmentation) with that in νp reactions [13] for the forward (⊕) and backward (□) hemispheres in the overall hadronic centre of mass.

Fig. 11 : Comparison of $\langle p_T^2 \rangle$ as a function of x_F for this experiment (●) with the corresponding data in K^+p reactions (0) [4].

Fig. 12 : Energy flow in the event plane with respect to the sphericity axis for $\Sigma_i (p^i_{T_{in}})^2 > p^2_{T_{min}}$ where $p^2_{T_{min}}$ is successively 0, 1, 2, 3 $(GeV/c)^2$.

Fig. 13 : Relative number of particles on one side of the sphericity axis for the same cuts as in Fig. 12.

Fig. 14 : The p_T^2 distribution of single particle jets. The solid curve corresponds to the higher-twist contribution of Fig. 4, normalized to the data. The broken curve corresponds to the high-z fragmentation of the minimum-twist contributions of Figs. 1 and 2 normalized relative to the higher-twist contribution.

Fig. 15 : As Fig. 14.

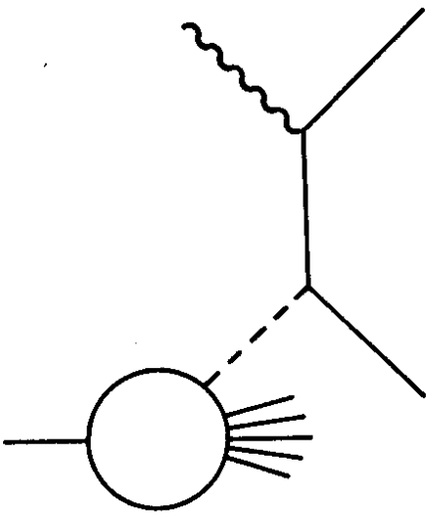

Fig. 1

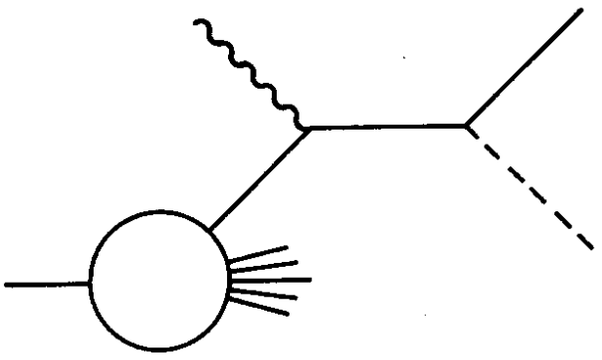

Fig. 2

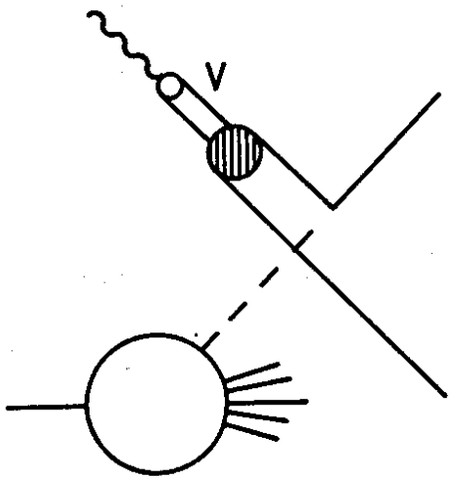

Fig. 3

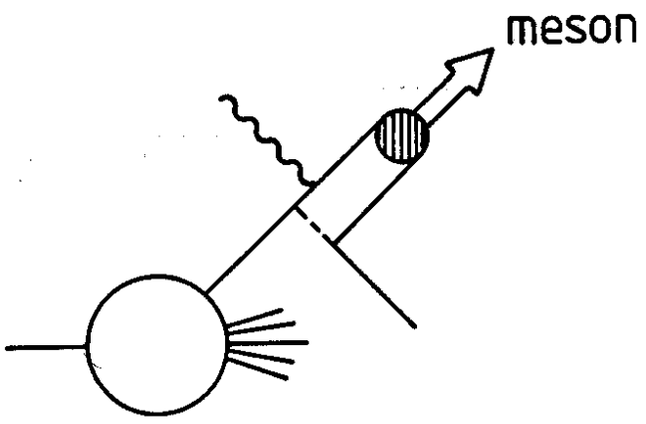

Fig. 4

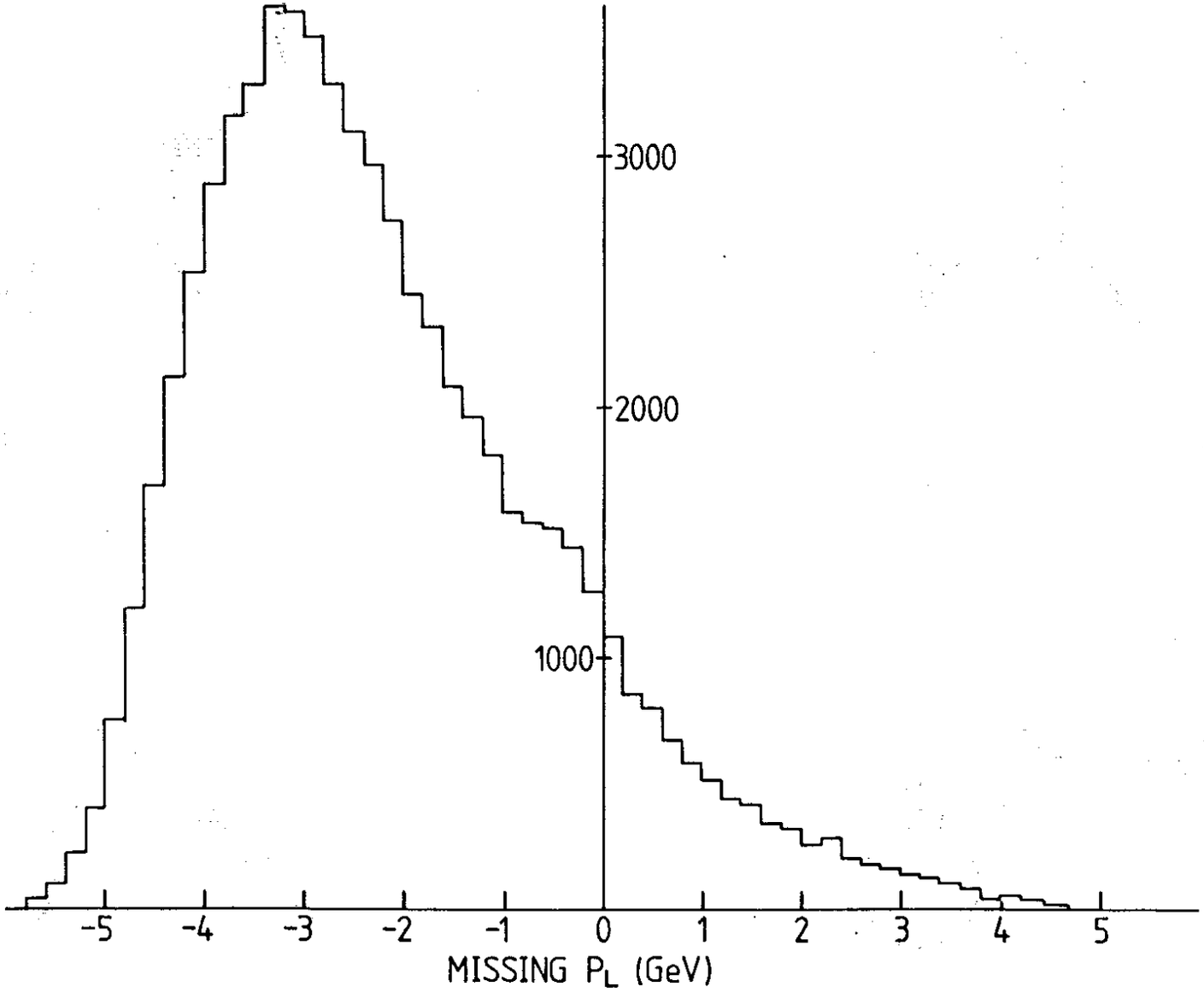

Fig. 5

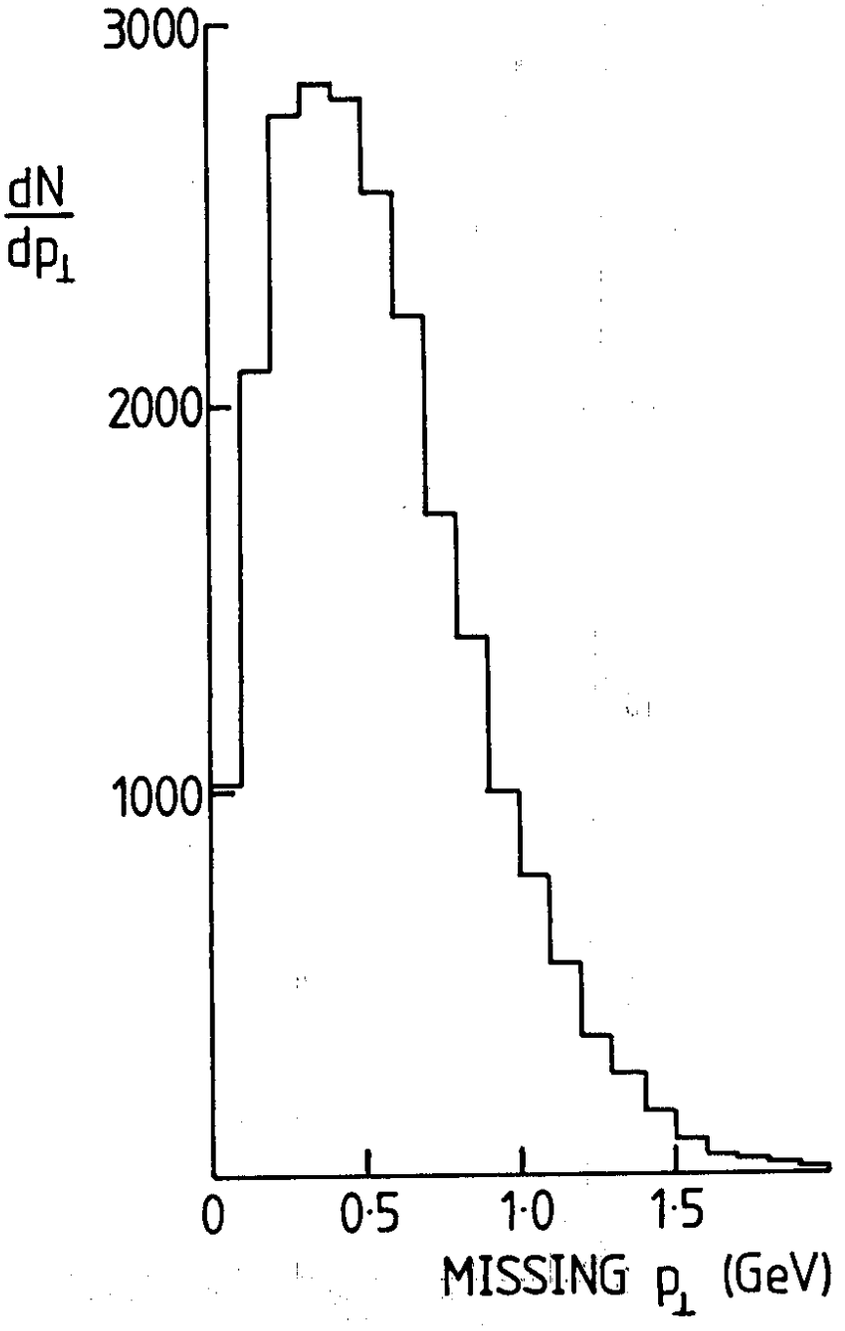

Fig. 6

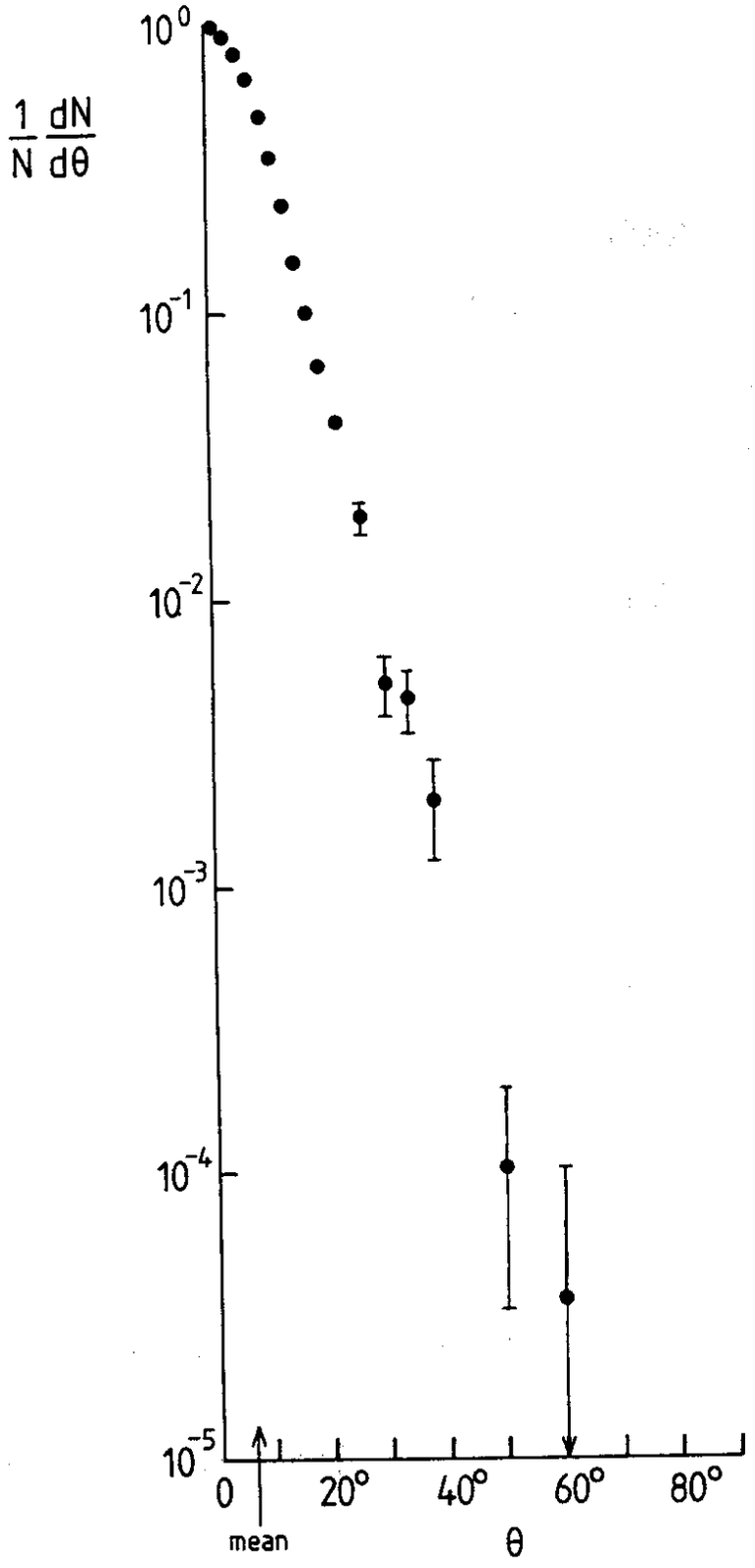
$\frac{1}{N}\frac{dN}{d\theta}$
10^{0}
10^{-1}
10^{-2}
10^{-3}
10^{-4}
10^{-5}
0
20°
40°
60°
80°
mean
θ

Fig. 7

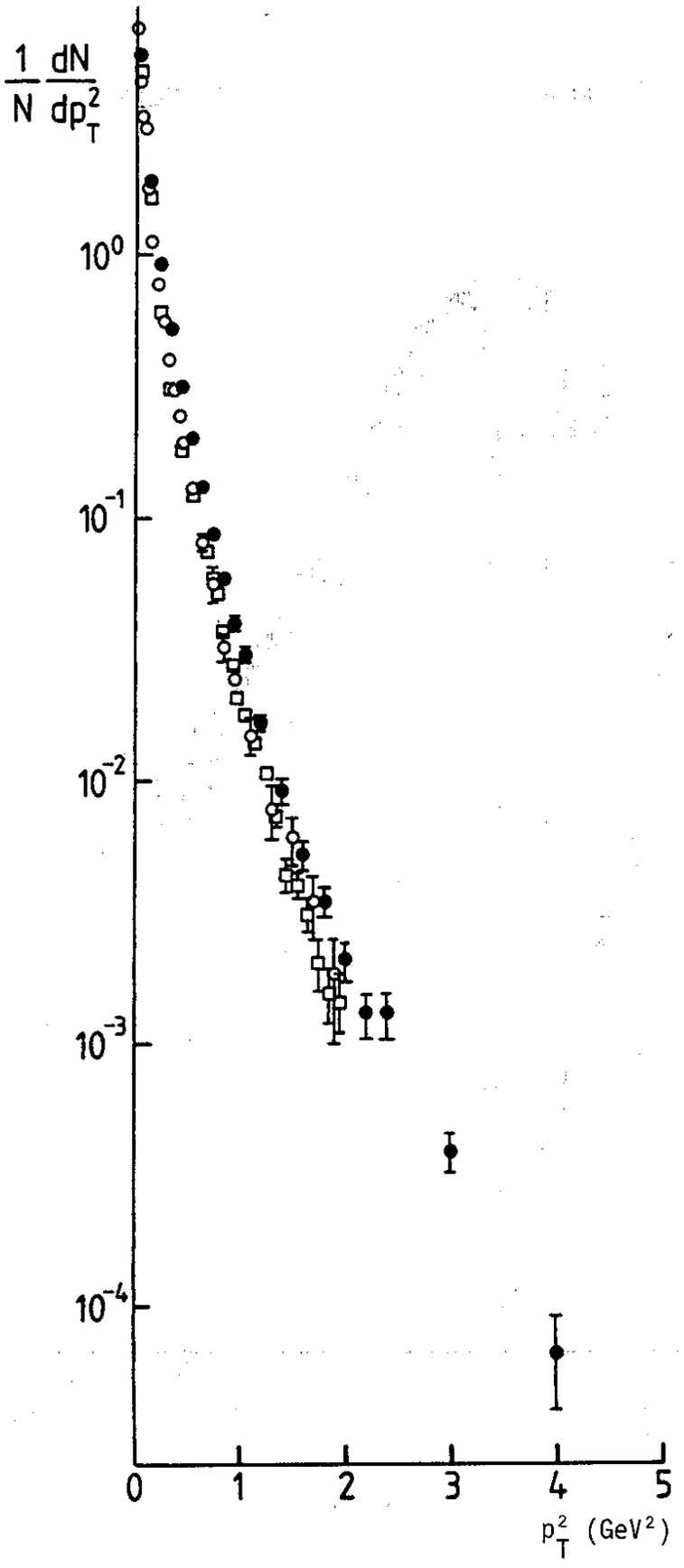

Fig. 8

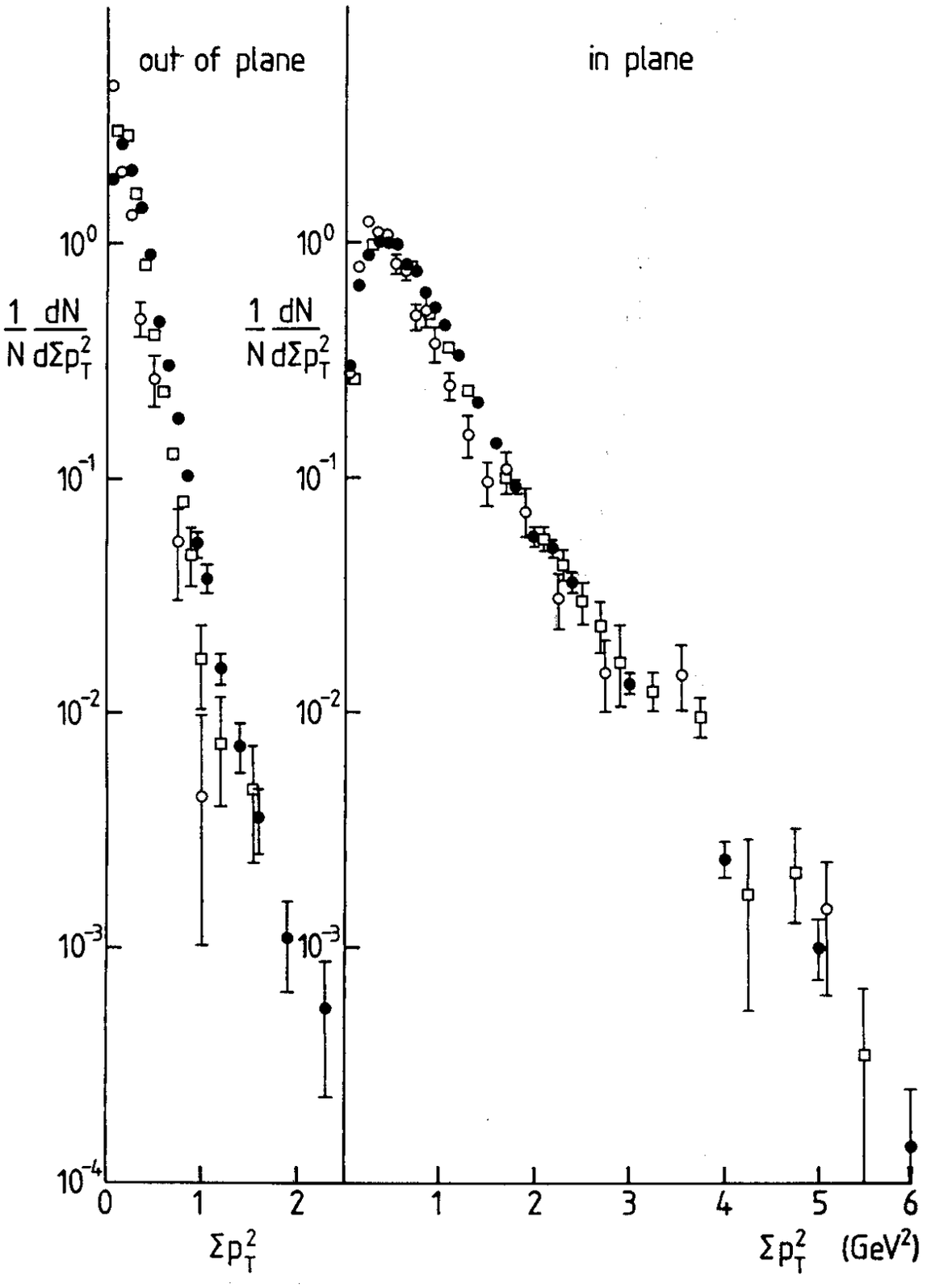
out of plane
in plane
$\frac{1}{N}\frac{dN}{d\Sigma p_T^2}$
10^0
10^{-1}
10^{-2}
10^{-3}
10^{-4}
0
1
2
3
4
5
6
Σp_T^2
Σp_T^2 (GeV^2)

Fig. 9

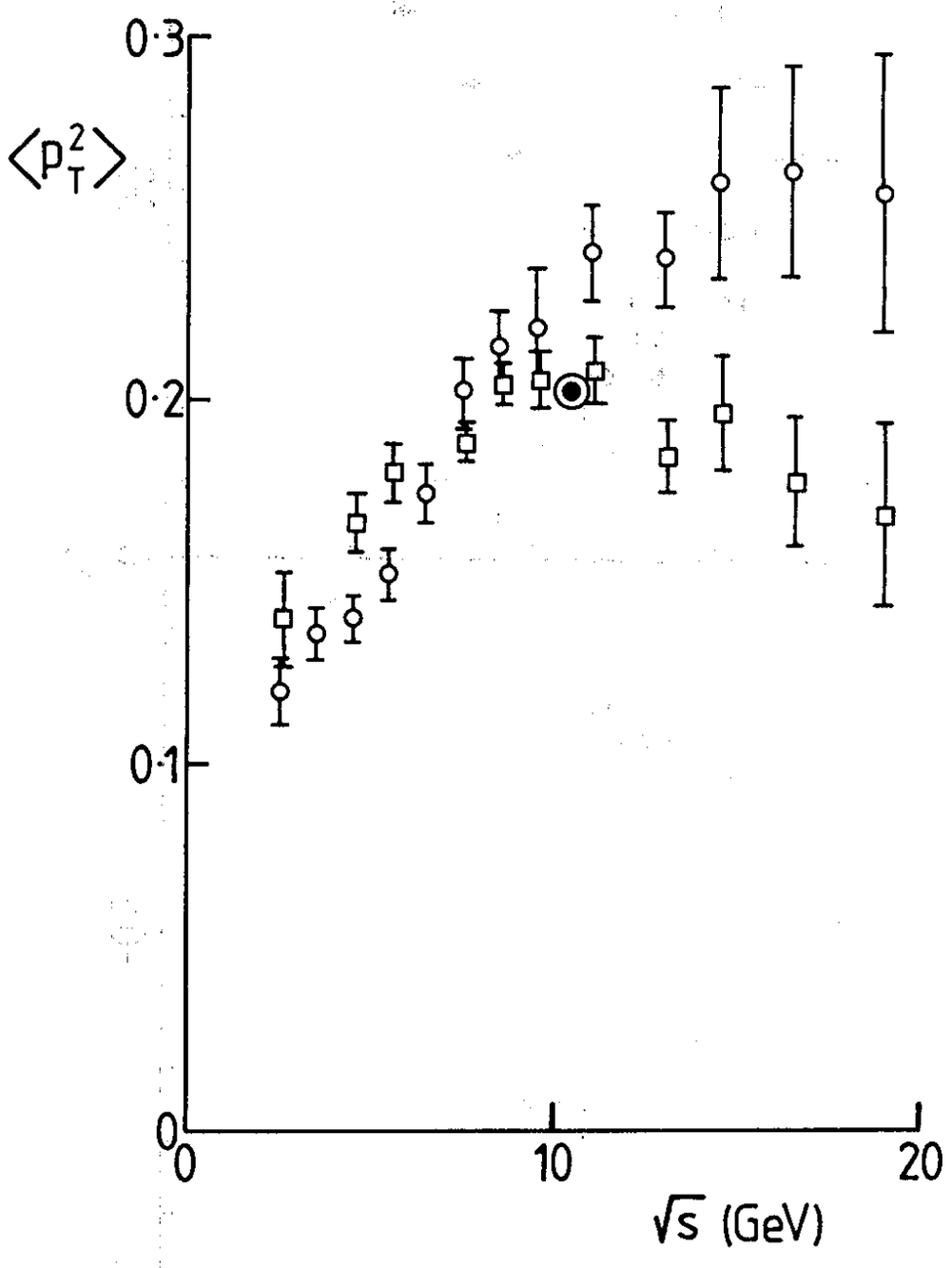

Fig. 10

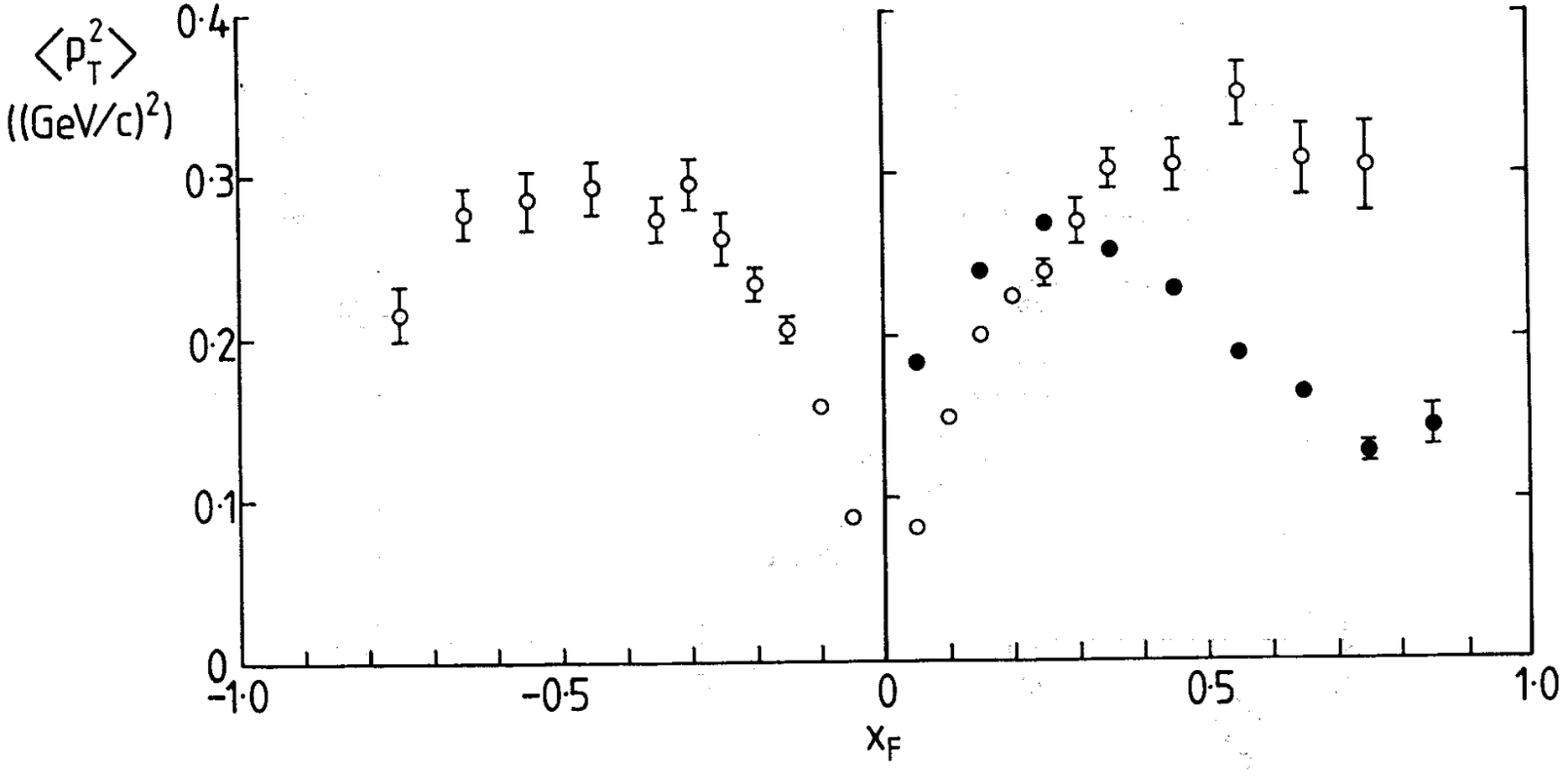

Fig. 11

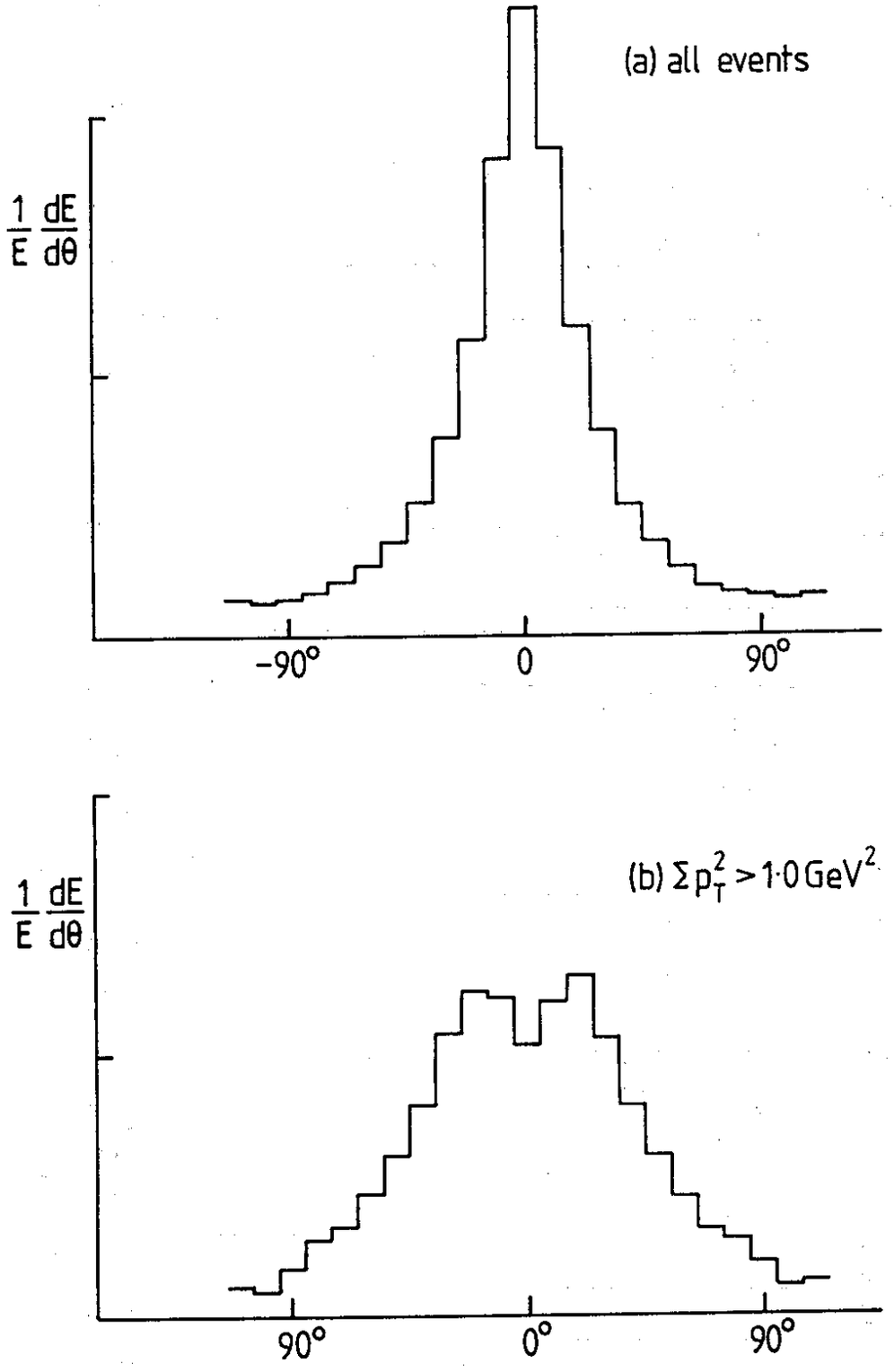
(a) all events
$\frac{1}{E}\frac{dE}{d\theta}$
-90°
0
90°
(b) $\Sigma p_T^2 > 1{\cdot}0\,GeV^2$
$\frac{1}{E}\frac{dE}{d\theta}$
90°
0°
90°

Fig. 12

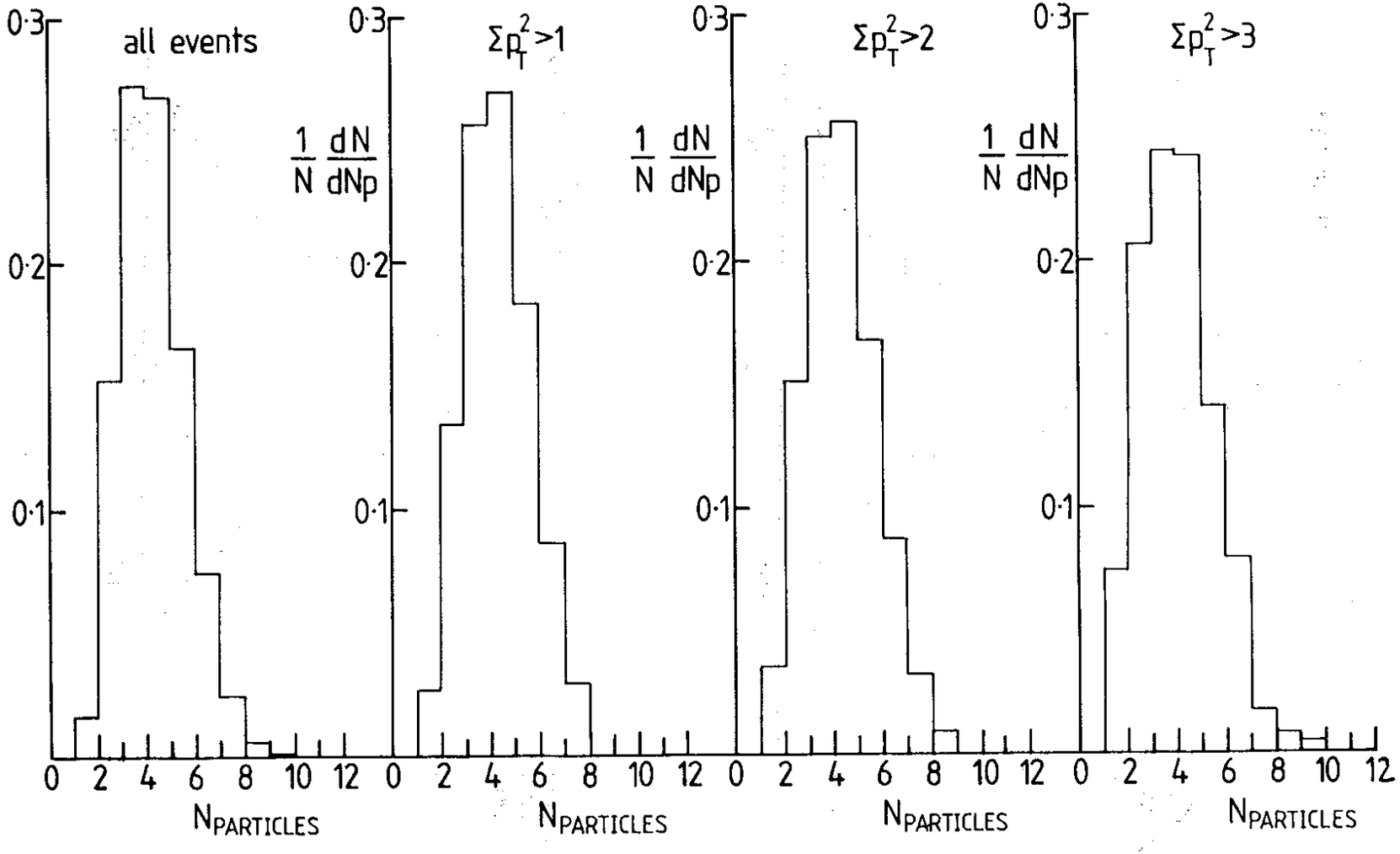
all events
$\Sigma p_T^2 > 1$
$\Sigma p_T^2 > 2$
$\Sigma p_T^2 > 3$
$\frac{1}{N}\frac{dN}{dNp}$
0·3
0·2
0·1
0 2 4 6 8 10 12
$N_{PARTICLES}$

Fig. 13

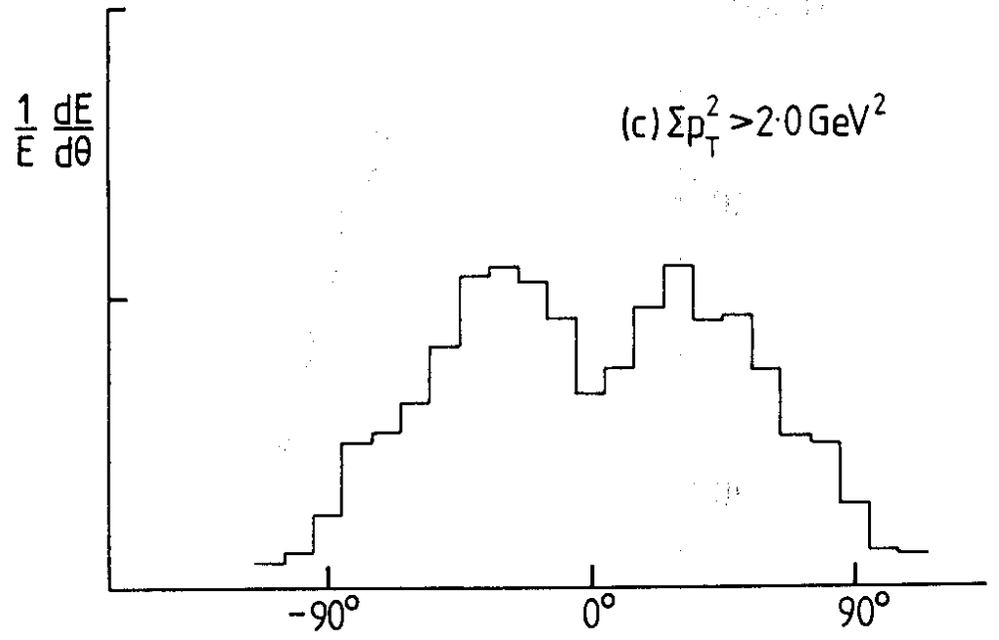
$\frac{1}{E}\frac{dE}{d\theta}$
(c) $\Sigma p_T^2 > 2{\cdot}0\,GeV^2$
-90°
0°
90°

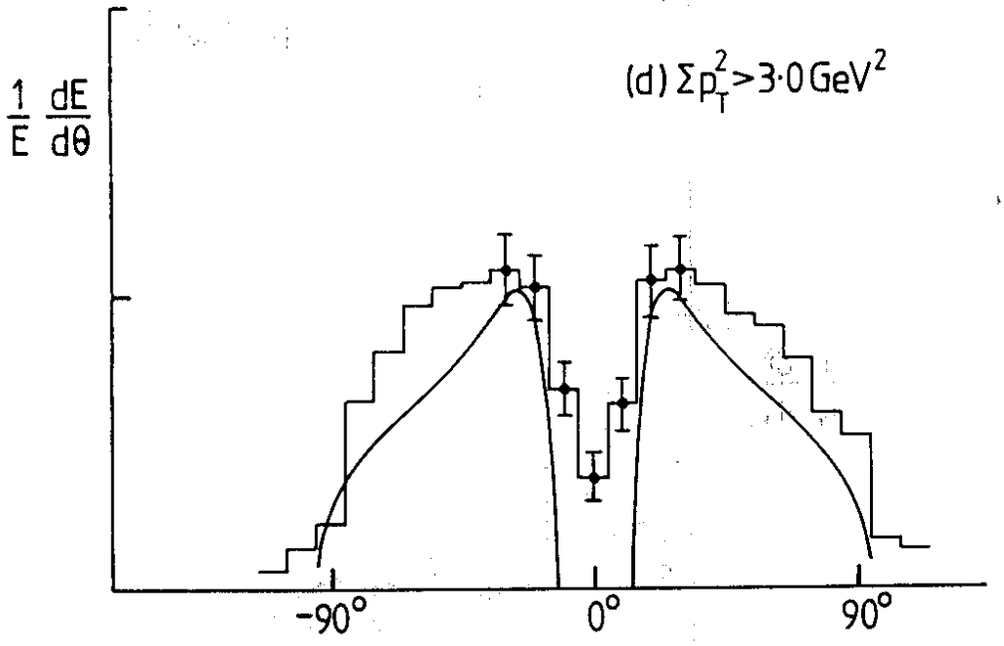
$\frac{1}{E}\frac{dE}{d\theta}$
(d) $\Sigma p_T^2 > 3{\cdot}0\,GeV^2$
-90°
0°
90°

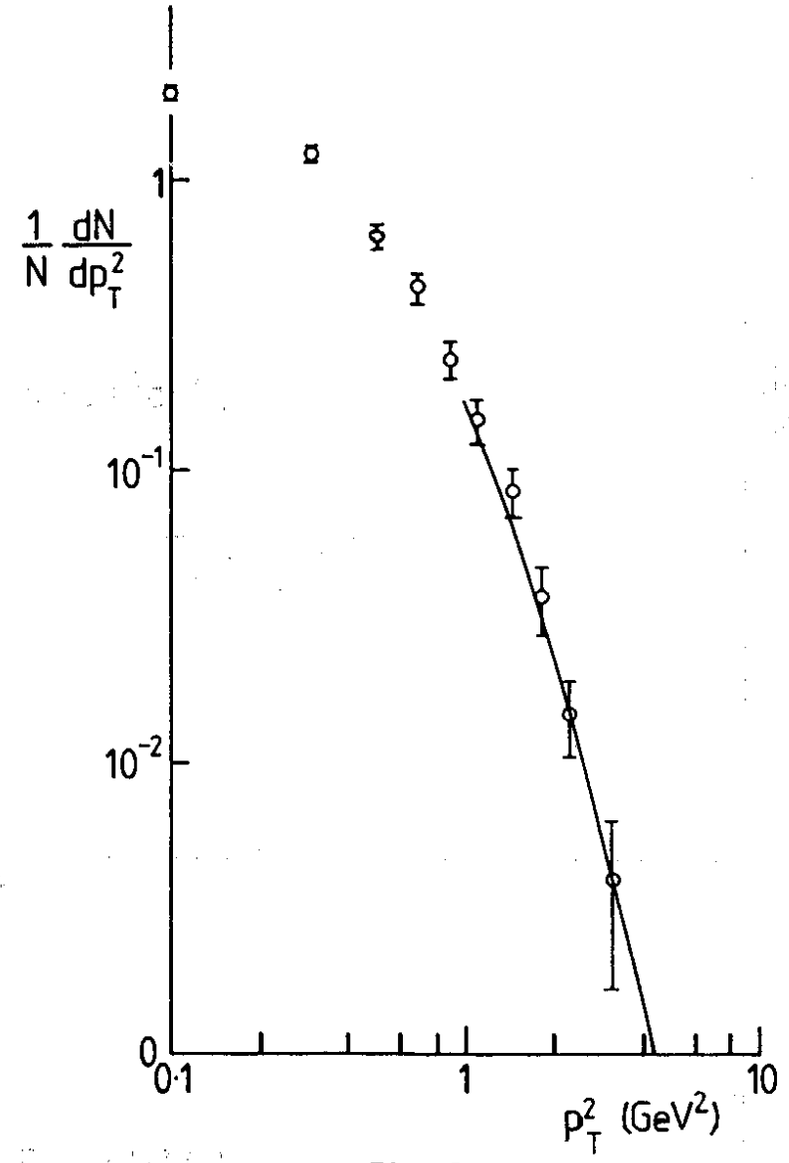

Fig. 14

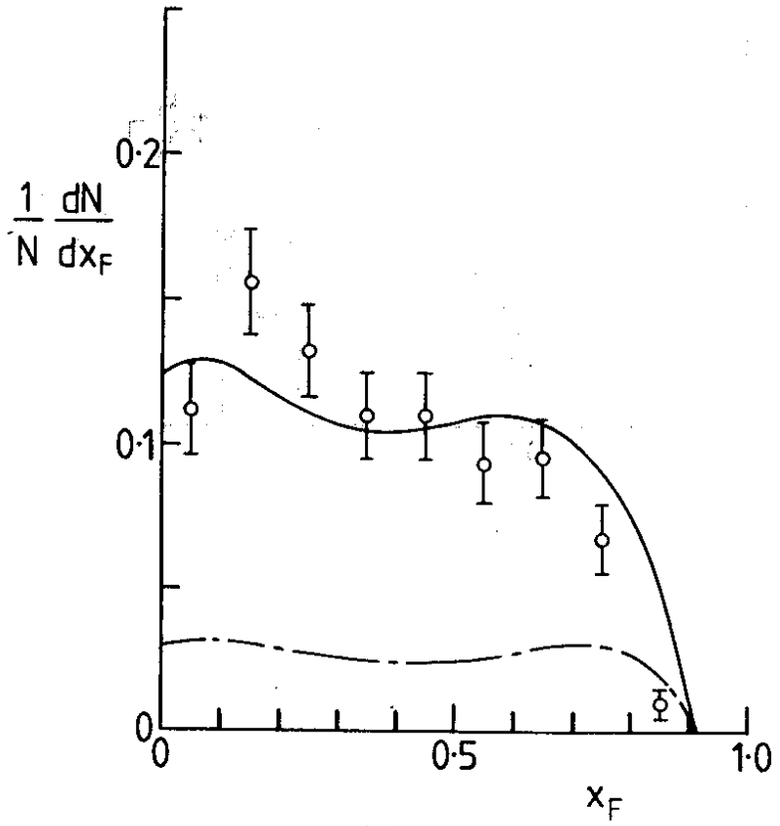

Fig. 15